

Mechanics of smart origami sunscreens with energy harvesting ability

Raffaele MIRANDA^{1*}, Enrico BABILIO², Narinder SINGH¹, Filipe SANTOS³, Fernando FRATERNALI¹

¹Department of Civil Engineering, University of Salerno, via Giovanni Paolo II, 132, 84084, Fisciano (SA), Italy

²Department of Structures for Engineering and Architecture (DiSt), University of Naples "Federico II", via Forno Vecchio 36, 80134, Naples, Italy

³CERIS and Departamento de Engenharia Civil da Faculdade de Ciências e Tecnologia da Universidade Nova de Lisboa, Quinta da Torre, Caparica, Portugal

*Corresponding author ramiranda@unisa.it
Tel.: 089/964083

Abstract

Recent studies have investigated the use of origami sunscreens with tensegrity architecture for the design of active solar façades of energy efficient buildings. This paper presents a mechanical study on the dynamic response of shading screens that are formed by origami panels activated through the tensioning and relaxation of selected strings. The basic module of the examined screens includes tensegrity units with displacement amplification properties that are equipped with piezoelectric cables. A numerical procedure for the simulation of the dynamic response of the examined sunscreens under arbitrary loading is formulated. The proposed model is employed to study the actuation motion exhibited by the elementary origami module, and its vibrations under the action of wind forces. The peculiar ability of tensegrity shading systems to harvest the mechanical energy stored in the strings is investigated, by drawing comparison with the energy harvesting abilities of photovoltaic panels and microeolic turbines.

© 2019 The Authors. Published by Elsevier Ltd.

Keywords: tensegrity structures; dynamic solar façades; energy efficient buildings; energy harvesting

1. Introduction

A high energy efficiency building is “a construction capable of ensuring a well-being condition within it by minimizing the use of non-renewable energy sources” [1]. The 2010 Energy Performance of Buildings Directive (EPBD) [2] made nearly zero-energy buildings (nZEB) the required norm for the design of new buildings in the EU from 2021. According to the EU Horizon 2020 program for research and innovation, one of the most relevant components of energy efficient buildings is the building envelope [3]-[5]. This component must meet more functions than just the separation of the outer space from the interior of the building, such as, e.g., providing sufficiently high thermal insulation, in order to minimize the energy consumption due to air conditioning.

Smart adaptive façades are designed to adapt to the external environment, and are often placed at a reasonable distance from the indoor areas [6],[7]. Regardless of whether such façades are part of the primary load bearing structure or not, their presence may significantly affect the overall structural behaviour of the building, especially under the action of wind forces [8].

Recent studies have proposed the use of tensegrity systems [9]-[12] for the design of dynamic envelopes of buildings with morphing behavior, thanks to the special deployment ability of such structures [13]-[14]. The opening/closure of the units of these sunscreens is conveniently activated by controlling the

elongation of a limited number of strings [13]. The use of tensegrity structures as renewable energy harvesters awaits attention. It was first proposed by Skelton and de Oliveira [9], in order to design of a station-keeping buoy that is able to convert ocean wave motion into electrical energy.

This paper deals with a reformulation of the design of the origami sunscreens with tensegrity architecture recently proposed to form the dynamic envelopes of the Al Bahar Towers in Abu-Dhabi [15],[16]. A new design of the tensegrity Al Bahar screens (TABS) studied in [14] is carried out (Sect. 2), in order to develop novel dynamic sunscreens with wind and actuation energy harvesting ability, which are referred to as WTABS throughout the paper. Three-dimensional D-bar elements [9] are added to the TABS modules, with the aim of profiting from the displacement amplification properties of such structures [9]. A numerical model is formulated (Sect. 3) for the simulation of the WTABS dynamics under the actuation motion and the action of wind forces (Sect. 4). The proposed model assumes that the compressive members (i.e., the bars) of the WTABS module respond as rigid bodies, while the tensile members (cables or strings) respond as elastically deformable elements. The transformation of the mechanical energy stored in the strings into electrical power is analyzed. The given results show that the WTABS can act as lightweight and cost-effective shading systems, with peculiar energy harvesting abilities (Sects. 5, 6). The novelty of the research presented in

this work with respect to the study presented in Ref. [14] is manifold and refers the following points: *i)* the addition of energy harvesting units to the TABS module studied in [14], which leads us to the design of the new module labeled WTABS; *ii)* the extension of the static analysis presented in Ref. [14] to the dynamic regime, through an in-house developed numerical model (Sect. 3.1); *iii)* the inclusion of a dynamical modeling of wind forces acting on the analyzed screens (Sect. 3.2); and *iv)* the development of a detailed study about the energy harvesting ability of the WTABS module (Sect. 5).

2. WTABS layout

The basic module of the WTABS examined in the present study enriches the TABS unit studied in [14], due to the addition of a set of six D-bar systems acting as mechanical energy harvesters. The original TABS system is graphically illustrated in Fig. 1. It is composed of ‘origami’ (umbrella shaped) eyes, whose unit cell (or basic module) consists of a tensegrity structure formed by 12 bars and 3 perimeter strings. The activation motion of each module is controlled by stretching and relaxing the perimeter strings, which leads to suitably tune the geometric stiffness of the structure [13]. The module is made up of a macro-triangle anchored parallel to the building façade, which is subdivided into six micro-triangles. The latter are able to move rigidly in space according to a morphing-type behaviour, thereby ensuring minimal internal energy storage in the deployment phase.

The elementary module of the WTABS system is shown in Fig. 2(b,c). Fig. 2(b) details the six D-bar units added to the TABS module of Fig. 2(a), while Fig. 2(c) shows the overall WTABS module. The actuation of such a structure is powered by a linear actuator Rolaram® R2501190 (294 kN dynamic loading, 3500 mm maximum stroke [17]), which is positioned at a vertex of the module. The actuator stretches and relaxes the external cables (see Fig. 2(b)), thus activating the unfolding/folding mechanism of the system. A telescopic collar guides the movement of the infill panels along the z axis, orthogonally to the building’s façade (Fig. 3). Two linear springs with stiffness constant $K = 67 \text{ kN m}^{-1}$ control the in-plane displacements of the other two vertices of the structure. The module employs 6082-T5 Aluminum bars and nylon fiber ropes as strings, which are subject to axial strains up to $\approx 15\%$ [14].

The total weight of the original TABS module is approximately equal to 7.40 kN, including structural parts (about 3.00 kN), PTFE (glass fiber) infill panels (0.13 kN), and the linear actuator (4.23 kN). Such a weight is approximately equal to one half of that of the sunscreens designed by Aedas architects for the Al Bahar towers [15]-[16]. The height of the module is equal to 4200 mm, while its width ranges between 3600 mm and 5400 mm. The bars of the WTABS module are made of the 6082-T5 Aluminum alloy, while the strings have a composite architecture, being formed by a central nylon cable coated by a bundle of Polyvinylidene Fluoride (PVDF) piezoelectric cables [18]-[19]. We refer the reader to Sect. 4

for the overall mass analysis of the WTABS module, and the mechanical properties of its components.



Fig. 1. Illustration of the TABS design for the origami sunscreens of the Al Bahar Towers in Abu Dhabi [14].

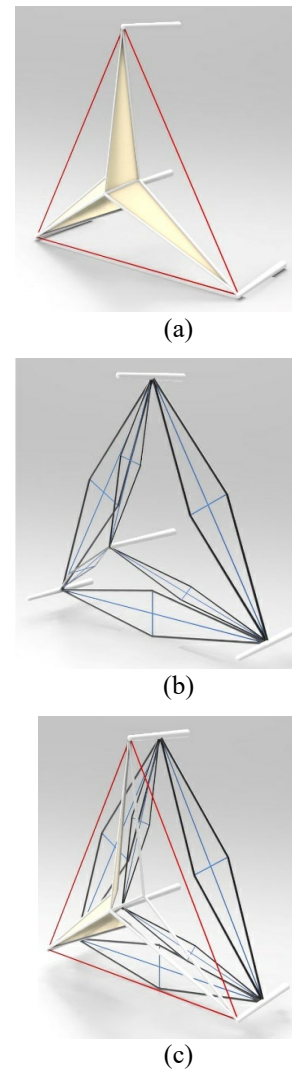


Fig. 2. Illustration of the WTABS model: (a) elementary TABS module; (b) D-bar elements with mechanical energy harvesting abilities; (c) overall WTABS module.

3. Mechanical modeling of the WTABS dynamics

The present section illustrates a numerical model for the simulation of the dynamic response of the WTABS structural system, through a Runge-Kutta approach to the time-integration of the competent equations of motion [20] (Sect. 3.1). The employed procedure suitably generalizes that

presented in Refs. [20],[21], in order to account for the presence of wind forces (Sect. 3.2).

3.1 Equations of motion

Throughout the paper, we indicate matrices with bold capital letters (i.e. \mathbf{X}), vectors with bold lower case letters (i.e. \mathbf{x}), and scalars with italic letters (i.e. x). The examined mechanical model describes the bars as rigid members and the strings as elastically deformable elements. It is composed of n_n nodes (or joints), n_b bars and n_s strings (or cables), and makes use of the following basic assumptions:

- the strings act as straight elastic springs that can carry only tensile forces (no-compression response);
- the bars behave as straight rigid bodies with uniform mass density, constant cross-section, and negligible rotational inertia about the longitudinal axis [20];
- the nodes consist of frictionless ball joints;
- duplicated nodes are introduced in correspondence of junctions attached to more than one bar (one node for each bar), which are constrained to move jointly in space [20].

Let $\mathbf{n}_i \in \mathbb{R}^3$ denote the generic node in the three-dimensional Euclidean space ($i \in [1, \dots, n_n]$). We describe the positions of all the nodes through the following node matrix

$$\mathbf{N} = [\mathbf{n}_1 \ \mathbf{n}_2 \ \dots \ \mathbf{n}_i \ \dots \ \mathbf{n}_{n_n}] \in \mathbb{R}^{3 \times n_n} \quad (1)$$

The external force vector acting on the generic node is described by the vector $\mathbf{w}_i \in \mathbb{R}^3$, while the overall loading condition applied to the structure is described by the following load matrix

$$\mathbf{W} = [\mathbf{w}_1 \ \mathbf{w}_2 \ \dots \ \mathbf{w}_i \ \dots \ \mathbf{w}_{n_n}] \in \mathbb{R}^{3 \times n_n} \quad (2)$$

We let \mathbf{b}_k , \mathbf{s}_k , \mathbf{r}_k respectively denote the vector joining the end nodes of the generic bar, the vector joining the end nodes of the generic string and the position vector of the center of mass of the generic bar. The following matrices group all such vectors

$$\mathbf{B} = [\mathbf{b}_1 \ \mathbf{b}_2 \ \dots \ \mathbf{b}_k \ \dots \ \mathbf{b}_{n_b}] \in \mathbb{R}^{3 \times n_b} \quad (3)$$

$$\mathbf{S} = [\mathbf{s}_1 \ \mathbf{s}_2 \ \dots \ \mathbf{s}_k \ \dots \ \mathbf{s}_{n_s}] \in \mathbb{R}^{3 \times n_s} \quad (4)$$

$$\mathbf{R} = [\mathbf{r}_1 \ \mathbf{r}_2 \ \dots \ \mathbf{r}_k \ \dots \ \mathbf{r}_{n_n}] \in \mathbb{R}^{3 \times n_n} \quad (5)$$

Upon introducing the connectivity matrices of bars ($\mathbf{C}_B \in \mathbb{R}^{n_b \times n_n}$), cables ($\mathbf{C}_S \in \mathbb{R}^{n_s \times n_n}$) and centers of mass ($\mathbf{C}_R \in \mathbb{R}^{n_b \times n_n}$), one easily obtains

$$\mathbf{B} = \mathbf{N} \mathbf{C}_B^T, \quad (6)$$

$$\mathbf{S} = \mathbf{N} \mathbf{C}_S^T, \quad (7)$$

$$\mathbf{R} = \mathbf{N} \mathbf{C}_R^T \quad (8)$$

It is useful to observe that the generic element C_{Bij} (or C_{Sij}) is equal to -1 if \mathbf{b}_i (or \mathbf{s}_i) is directed away from node j ; 1 if such a vector is directed towards such a node, and 0 if \mathbf{b}_i (or \mathbf{s}_i) does not touch node j . According to the classification introduced in [9], a tensegrity system is said of class m , if the maximum

number of bars concurring in each node is equal to m . It is an easy task to verify that the WTABS module in Fig. 2(b) is a tensegrity system of class 6.

We now introduce the force density (member force divided by length) of the k^{th} cable as it follows

$$\gamma_k = \left[0, k_k \left(1 - \frac{L_k}{s_k} \right) \right] + \gamma_{ck} \quad (9)$$

Here, k_k is the axial stiffness coefficient of the current string, L_k is its rest length, s_k is the current length, and γ_{ck} is the force density produced by damping effects. The latter is computed as [20],[21]

$$\begin{aligned} \gamma_{ck} &= c_k \dot{s}_k / s_k, \quad \text{if } s_k \geq L_k, \\ \gamma_{ck} &= 0, \quad \text{if } s_k < L_k. \end{aligned} \quad (10)$$

Under the above settings, we can write the equations of motion of the tensegrity system under examination as follows [20]

$$\dot{\mathbf{N}}\mathbf{M} + \mathbf{N}\mathbf{K} = \mathbf{W} \quad (11)$$

where

$$\mathbf{M} = \mathbf{C}_B^T \hat{\mathbf{m}} \mathbf{C}_B \frac{1}{12} + \mathbf{C}_R^T \hat{\mathbf{m}} \mathbf{C}_R \in \mathbb{R}^{n_n \times n_n} \quad (12)$$

$$\mathbf{K} = \mathbf{C}_S^T \hat{\boldsymbol{\gamma}} \mathbf{C}_S - \mathbf{C}_B^T \hat{\boldsymbol{\lambda}} \mathbf{C}_B \in \mathbb{R}^{n_n \times n_n} \quad (13)$$

Here, $\hat{\boldsymbol{\lambda}}$ is the force density vector of the bars defined by the following equation (Lagrange multiplier of the bar rigidity constraint [20],[21])

$$-\hat{\boldsymbol{\lambda}} = [\dot{\mathbf{B}}^T \dot{\mathbf{B}}] \hat{\mathbf{m}} \hat{\boldsymbol{\lambda}}^{-2} \frac{1}{12} + [\mathbf{B}^T (\mathbf{W} - \mathbf{S} \hat{\boldsymbol{\gamma}} \mathbf{C}_S) \mathbf{C}_B^T] \hat{\boldsymbol{\lambda}}^{-2} \frac{1}{2} \in \mathbb{R}^{n_b \times n_b} \quad (14)$$

where $\hat{\boldsymbol{\lambda}}^{-2} \in \mathbb{R}^{n_b \times n_b}$ is a diagonal matrix with entries $\hat{\lambda}_k^{-2} = \|\mathbf{b}_k\|^{-2}$, and the symbol $[\cdot]$ denotes the diagonal matrix that collects the diagonal entries of matrix $[\cdot]$. It should be noted that the stiffness matrix \mathbf{K} appearing in Eqn. (11) is not constant, being a function $\mathbf{K} = \mathbf{K}(t, \mathbf{N}, \dot{\mathbf{N}}, \hat{\boldsymbol{\gamma}})$ of time and the mechanical variables \mathbf{N} , $\dot{\mathbf{N}}$, $\hat{\boldsymbol{\gamma}}$.

We employ the fourth-order Runge-Kutta algorithm described in [20],[21] to integrate the equations of motion (11) from a given initial time t_0 to a final time t_f , using a small enough integration step dt .

3.2 Modelling of the wind forces

Wind is a natural phenomenon that consists of the movement of air masses due to the pressure difference between two points of the atmosphere. The instantaneous wind vector speed \mathbf{V} can be represented by the composition of the average speed \mathbf{V}_m over an interval of 10 minutes, and the turbulence term \mathbf{V}' , which accounts for high frequency fluctuations [22]

$$\mathbf{V}(P, t) = \mathbf{V}_m(P) + \mathbf{V}'(P, t) \quad (15)$$

$$\mathbf{V}_m(P) = \mathbf{k} v_m(y) \quad (16)$$

$$\mathbf{V}'(P, t) = \mathbf{i} v'_1(P, t) + \mathbf{j} v'_2(P, t) + \mathbf{k} v'_3(P, t) \quad (17)$$

In the above equations above, P is any point of the space, t is the time, \mathbf{i} , \mathbf{j} , \mathbf{k} are the unit vectors along the Cartesian axes x , y , z , such that z is perpendicular to the plane of the building façade; v_m is the average speed longitudinal at height y and v'_1 , v'_2 , v'_3 are the lateral (x), vertical (y) and longitudinal (z)

components of turbulence.

The following analysis considers only turbulent fluctuations v'_3 and assume that such fluctuations are representable as a single stationary Gaussian random process with zero mean, which depends only on the height and time, that is $v'_3(P,t)=v'(y,t)$. Such a random variable is described by the following spectral density [22]

$$S_L(y, n) = \frac{6.8 f_L(y, n)}{(1+10.2 f_L(y, n))^{5/3}} \quad (18)$$

where $f_L(y, n)$ is a dimensionless frequency

$$f_L(y, n) = \frac{nL(y)}{v_m(y)} \quad (19)$$

$L(y)$ being the turbulence scale, and n the natural frequency. By choosing a frequency step $\Delta n=0.05$ Hz, and a set of 100 frequencies $n_k=(k-1/2) \Delta n$, we obtain [8]

$$v'(y, t) = \sum_{k=1}^N \sqrt{2 S_L(y, n_k) \Delta n} \cos(2\pi n_k t + \varphi_k) \quad (20)$$

φ_k denoting randomly generated phase angles (in radians) over $0-2\pi$. Finally, we cast the peak value of the wind kinetic pressure (in m/s) into the following form

$$q_p(y, t) = \frac{1}{2} \rho (v_m(y) + v'(y, t))^2 \quad (21)$$

$\rho=1.25 \text{ kg m}^{-3}$ being the density of air.

The simulations presented in Sect. 4.3 employ numerical data corresponding to the height and the environmental conditions of the Al Bahar Towers. By setting $y^*=120$ m in a coastal area exposed to wind, we obtain the turbulence scale $L(y^*) = 40.1589$ m [22]. We consider the average velocity $v_m(y^*) = 73.4 \text{ m s}^{-1}$, which corresponds to the wind pressure of 3.5 kPa measured through tunnel tests on full-scale screen prototypes of the towers [16].

4. Numerical results

We deal in the present section with numerical simulations of the dynamics of a WTABS module under the actuation motion (Sect. 4.2) and wind-induced vibrations (Sect. 4.3). Our simulations consider a damping factor of 5%, a time step of 0.025 s, and the material properties that are illustrated in the following section.

4.1 Material properties and effective masses

The bars of the WTABS module employ the 6082-T5 Aluminum alloy, as in the TABS design presented in [14]. The strings make use of a wire rope featuring a nylon core cable with 8.9 mm diameter, which is helically wound with a bundle of piezoelectric coaxial cables [19]. The latter are obtained by covering lightweight conductive wires with PVDF films. The PVDF films are shrouded in a copper braid and cover central stretchable wires with 2.67 mm diameter. Such a composite structure is covered with a plastic coating for protection. A total of 42 piezoelectric cables is used to form the composite wire rope. The piezo cables are organized in 6 strands twisted around the nylon core, each of which shows 7 piezo cables, as

shown in Fig. 3. Using the Hruska's equation for the elastic response of a wire rope [23], and a 56 degree lay angle for the PVDF cables and the strands forming the rope, we predict an overall effective stiffness of the piezo-composite wire rope equal to 306.31 kN.

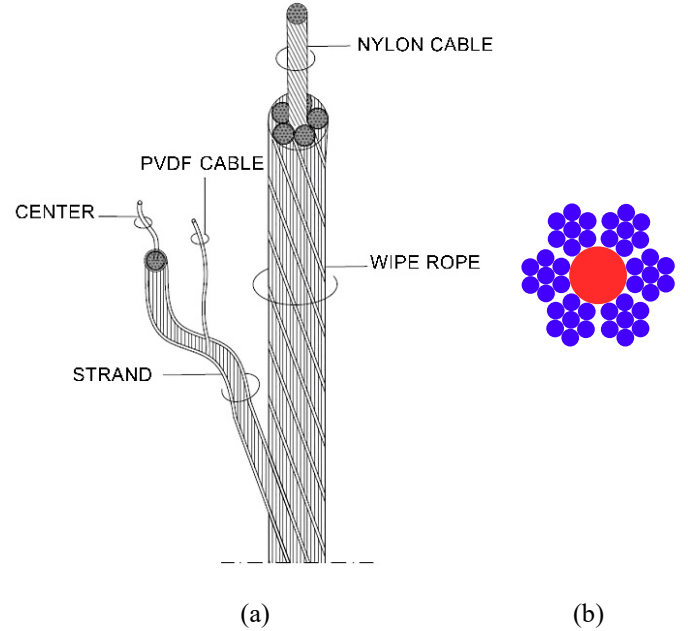


Fig.3. (a) Assembly of the composite wire rope used for the strings of the WTABS module. (b) Cross-section of the wire showing the nylon core (red) and the outer piezoelectric cables (blue).

The mechanical model introduced in the present work makes use of effective (equivalent) masses of the bars forming the WTABS module, which account for the actual masses of the bars, and a flat-rate calculation of the masses of nodes and the secondary structural elements (infill panels, made of PTFE coated fibre glass fabrics with 1.5 kg m^{-2} mass density per unit area, guiding rails, etc.). We compute the effective masses of the bars forming the outer triangles (see Fig. 2(a)) by doubling the masses of the 6082-T5 Aluminum bars, whose geometric and mechanical properties are listed in Table 1. We instead identify the effective masses of the 36 struts forming the 6 D-bar units placed behind the infill panels (see Fig. 2(c)) with the actual masses, since such bars are not connected to significant secondary structural elements. The effective masses given to all the bars of the WTABS module are listed in Table 2. The geometrical and mechanical properties of the strings are given in Table 3. The masses of the such elements are lumped at the nodes.

Table 1. Geometric and mechanical data of 6082-T5 Aluminum bars. The area of the cross sections is computed as $A_0=2 t (w+h-2 t)$.

Width	Height	Thickness	Material	Young modulus	Density
w	h	t		E	ρ
(mm)	(mm)	(mm)		(GPa)	(kg m^{-3})
150	70	5	6082-T5	72	2.70×10^3

Table 2. Effective masses of the bars.

# Element	Length (m)	Infill panel (kg)	Effective mass (kg)
3	1.3135	1.4941	16.3888
3	2.6269	1.4941	31.2836
6	2.2750	0.7470	26.5455
18	2.2755	-	12.9020
18	1.5966	-	9.0526

Table 3. Geometric and mechanical properties of the strings.

Diameter d (mm)	Material	Young modulus E_s (GPa)
9	Nylon core	3.9
2.67	Piezo cable	2.7 (PVDF film)

4.2 Simulation of the actuation motion

The opening and closure of the external macro-triangle forming the WTABS module is activated by a force applied to a vertex (actuated node) by the linear actuator Rolaram® R2501190 [14],[17]. The actuation motion deploys the screen from the open (folded) to the closed configuration over a time window of a 40 s. The closed configuration is almost (but not completely) flat, in order to avoid the penetration of the bars forming the macro-triangles [14].

We simulate the actuation motion by applying the above loading program to the numerical model presented in Sect. 3. The total simulation time is 80 s, since we hold the push force on the actuated node constant for 40 s, after the closure of the screen. At the initial time $t=0$ the force on the actuated node has the value $F_{\min}=72.690$ kN, which is necessary to apply the initial state of folding to the module [14]. At $t=40$ s, the actuation force reaches its maximum value, which is equal to $F_{\max}=276.221$ kN.

Fig. 4 and Fig. 5 illustrate three deformed configurations obtained through the numerical simulation of the actuation motion of the WTABS module, namely the initial state, an intermediate unfolded configuration reached at $t = 25$ s, and the deployed configuration occupied at $t = 50$ s (see the Appendix for an animation of the actuation motion). We assume that the actuated node is kept locked once the closed configuration has been reached. Fig. 4 also illustrates the time-history of the z -coordinate of the central node of the module during the actuation motion.

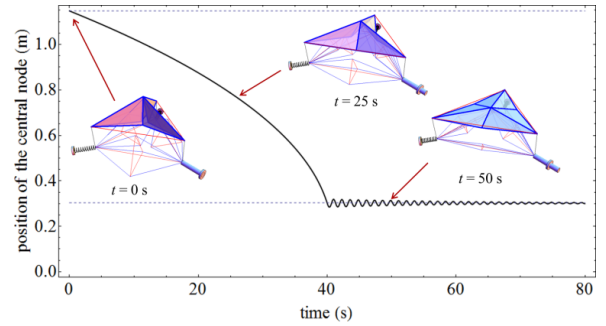


Fig. 4: Height of the central node vs time computed through the simulation of the actuation motion of the WTABS module.

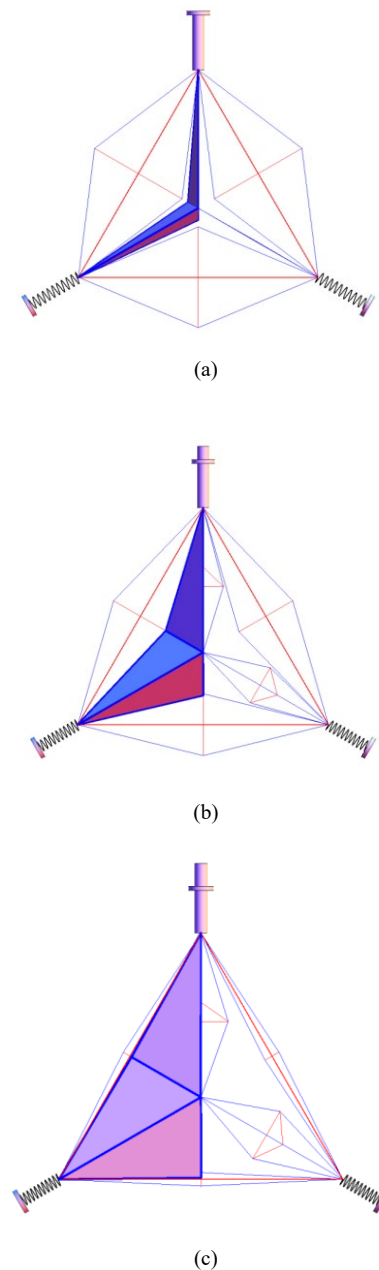


Fig. 5. Details of selected configurations of the actuation motion of the WTABS module: open configuration at $t = 0$ s (a), partially closed configuration at $t = 25$ s (b), and closed configuration at $t = 50$ s (c). The boundary springs and the actuator ram are idealized and not reported in scale. (see also the animation provided as supplementary material).

4.3 Simulation of the wind dynamics

The simulation of the wind dynamics of the WTABS module makes use of the modelling of the wind forces described in Sect. 3.2. Such forces are assumed to act on the closed configuration of the screen depicted in Fig. 5(c). We prescribe zero initial nodal velocities on such a configuration, since we assume that the actuator is locked under the action of wind forces. The total simulation time is set to 250 s. Fig. 6 illustrates the snapshot at $t=50$ s extracted from the simulation of the wind dynamics of the WTABS module (see the Appendix for an animation of such a simulation). Fig. 6 instead illustrates the time history of the z-coordinate of the central node of the module under the action of the wind forces.

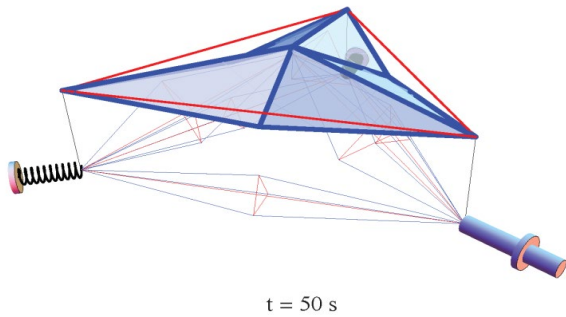


Fig. 6. Snapshots at $t=50$ s from the simulation of wind dynamics of the WTABS module. The boundary springs and the actuator ram are idealized and not reported in scale. (see also the animation provided as supplementary material).

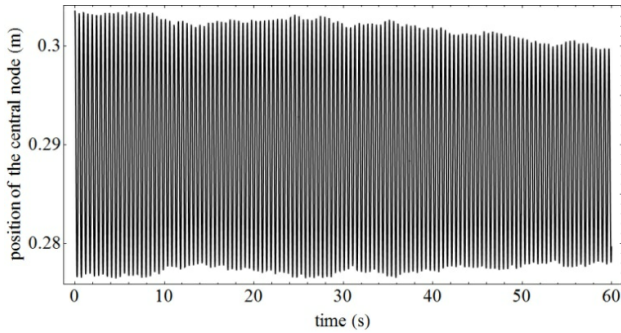


Fig. 7. Time history of the z-coordinate of the central node of the WTABS module along the direction normal to the building façade, during the first 60 s of the simulation.

5. Mechanical energy harvesting

The PVDF-coated piezoelectric cables composing the wire ropes of the WTABS module (Fig. 3) exhibit the mechanical properties listed in Table 4 (parameters imported from Refs. [24]-[25]). The elastic energy W_M stored into the piezoelectric cables is converted into electric energy W_E through the electromechanical effect described by the following equation (see [26], p. 21)

$$W_E = k_{33}^2 W_M \quad (22)$$

where k_{33} is the electromechanical coupling coefficient along the longitudinal axis of the piezoelectric cables.

We compute W_M by making use of the strain history recorded in the strings during the simulations of the actuation motion and the wind dynamics illustrated in Sect. 4, obtaining

$$W_M = \frac{1}{2T} \sum_{s=1}^{n_s} \left(E_f A_f L_{is} \int_0^T \varepsilon_s(t)^2 dt \right) \quad (23)$$

where T is the total time of simulation, L_{is} is the initial length of the s^{th} string, n_s is the number of strings, and A_f is the area of the PVDF film.

Table 4. Properties of the employed piezo cable.

Material	Young's modulus E_f (GPa)	Ultimate stress σ_f (MPa)	Ultimate strain ε_f (%)	Coupling coefficient k_{33} (-)
PVDF	2.7	350	16.9	0.15

With reference to the actuation motion analyzed in Sect. 4.2, Eqns. (22) -(23) allow us to predict the following overall values of the mechanical energy stored in the strings (W_M^{act}), and the electric energy produced through piezoelectric effect (W_E^{act})

$$W_M^{act} = 14082.1 \text{ kJ} = 3911.7 \text{ Wh}, \quad (24)$$

$$W_E^{act} = 321.3 \text{ kJ} = 89.2 \text{ Wh}. \quad (25)$$

A similar procedure leads us to predict the mechanical energy stored in the strings (W_M^{wind}) and the electric energy produced through piezoelectric effect (W_E^{wind}), in correspondence with the wind motion that has been studied in Sect. 4.3

$$W_M^{wind} = 25.548 \times 10^{-2} \text{ kJ} = 7.095 \times 10^{-2} \text{ Wh}. \quad (26)$$

$$W_E^{wind} = 5.749 \times 10^{-4} \text{ kJ} = 1.5968 \times 10^{-4} \text{ Wh}. \quad (27)$$

It is worth comparing the above energies with those that can be produced by photovoltaic panels and wind turbines available in the market. With reference to average values of the energies that can be produced over a day, Table 5 compares the electric energies per unit area produced by a WTABS module with the analogous energies that can be produced by photovoltaic (PV) panels in the area of Abu Dhabi (estimated through the PVWatts® calculator [31]) and by the microeolic wind turbines studied in [32] (rooftop setup). One observes that the energy that can be harvested per unit surface during the opening and closure of the WTABS is equal to about 3% and 1% of the energies that can be daily produced by PV panels and wind turbines, respectively. It is worth noting that the sunscreens of the Al Bahar towers include more than 1000 modules, each of which has a surface area of 8.75 m² [15]-[16]. The overall electric energy that can be daily produced by the WTABS actuation is therefore considerable, being approximately equal to that produced by 233 PV panels and 87 microeolic rooftop turbines with 1 m² surface area.

Table 5. Comparison of the electrical energies per unit surface that can be daily produced by different energy harvesting systems.

WTABS actuation	20 Wh m ⁻²
WTABS wind	0.263 mWh m ⁻²
PV panels	750 Wh m ⁻²
Wind turbines	2000 Wh m ⁻²

The results in Table 5 also show that one WTABS module is able to produce about 2.3 milliwatt hour under the action of wind forces, which is sufficient to power, e.g., microelectronic devices, WiFi repeaters, cellular phones, and/or LED lighting

systems [27].

6. Concluding remarks

Tensegrity structures have a special ability to act as lightweight deployable systems with “morphing” abilities [13]–[14],[28]–[30]. Making use of tensegrity concepts, we have generalized the design of the TABS sunscreens recently proposed in [14], in order to endow such structures with mechanical energy harvesting ability. We have proposed novel sunscreens, named WTABS, whose unit cell is obtained by complementing the TABS module with a set of D-bar units placed in the space running between the screens and the building façade. We have simulated the dynamics of the WTABS module in correspondence with the actuation motion and wind forces, making use of a mixed, rigid body (bars) – elastic springs (strings) mechanical model.

The results presented in Sect. 5 have led us to predict the amount of mechanical energy that can be harvested through piezoelectric effects by the WTABS structures. It has been shown that each of the sunscreens protecting the Al Bahar towers can daily produce a quantity of electric energy equal to that produced by about 233 m² of PV panels and 87 m² of rooftop wind turbines, due do the electromechanical conversion of the energy stored in the piezoelectric cables during the actuation motion. The energy that can be harvested under the action of wind forces is markedly lower, being however sufficient to power microelectronic devices and wireless systems [27].

Future directions of the present study will be addressed to the design of dynamic deployable structures supporting hybrid double-skin façades, which couple natural or mechanical ventilation systems with adaptive shading technologies. We also plan to investigate the use of different piezoelectric materials, such as piezoceramics, composites, polymers and monocrystals [18]–[19], through future work, in order to improve and optimize the energy harvesting capacity of the WTABS shading system.

Acknowledgements. RM, NS and FF gratefully acknowledge financial support from the Italian Ministry of Education, University, and Research (MIUR) under the ‘PRIN 2017’ Grant “Multiscale Innovative Materials and Structures”.

Appendix A. Supplementary material

Animations of the WTABS dynamics under the actuation motion and the action of wind forces can be found in the online version.

References

- [1] Herzog, T., Flagge, I., Herzog-Loibl, V., Meseure, A., Architekturmuseum, D.: Thomas Herzog: Architektur + Technologie. Architecture Series. Prestel (2001).
- [2] Directive 2010/31/EU of the European Parliament and of the Council of 19 May 2010 on the energy performance of buildings.
- [3] Pérez-Lombard, L., Ortiz, J., Pout, C.: A review on buildings energy consumption information. *Energy and Buildings* 40(3), 394–398 (2008). DOI 10.1016/j.enbuild.2007.03.007.
- [4] Alotaibi F (2015) The Role of Kinetic Envelopes to Improve Energy Performance in Buildings. *J. Archit. Eng. Tech.* 4: 149. doi:10.4172/2168-9717.1000149.
- [5] European Commission, HORIZON 2020 Work Programme 2014–2015, PART 5.ii, p. 98, 2014.
- [6] D. McFarquhar. The role of the building facade - Curtain walls, in: Proceedings of the BEST3 - Building Enclosure Science & Technology Conference. (www.briqbase.org/content/role-building-fa%C3%A7ade-%E2%80%93curtain-walls).
- [7] C. Bedon, X. Zhang, F. Santos, D. Honfi, M. Kozłowski, M. Arrigoni, L. Figuli, D. Lange, Performance of structural glass facades under extreme loads – Design methods, existing research, current issues and trends, *Constr. Build. Mater.* 163 (2018) 921–937.
- [8] Santos, Filipe & F. Goncalves, Pedro & Cismasiu, Corneliu & Mauricio, Gamboa-Marrufu. (2014). Smart glass façade subjected to wind loadings. *Structures & Buildings*. 167. 10.1680/stbu.13.00011.
- [9] Skelton, R., de Oliveira, M.: Tensegrity Systems. Springer US (2010).
- [10] K. Nagase, T. Yamashita, N. Kawabata, On a connectivity matrix formula for tensegrity prism plates, *Mechanics Research Communications*, Volume 77, 2016, Pages 29–43, doi.org/10.1016/j.mechrescom.2016.08.003.
- [11] Xian Xu, Sili Li, Yaozhi Luo, Form-finding of a new kind of tensegrity tori using overlapping modules, *Mechanics Research Communications*, Volume 84, 2017, Pages 1–7, doi.org/10.1016/j.mechrescom.2017.05.011.
- [12] Heping Liu, Jingyao Zhang, Makoto Ohsaki, 3-bar tensegrity units with non-equilateral triangle on an end plane, *Mechanics Research Communications*, Volume 92, 2018, Pages 124–130, doi.org/10.1016/j.mechrescom.2018.08.003.
- [13] Fraternali, F., De Chiara, E., Skelton, R.: On the use of tensegrity structures for kinetic solar facades of smart buildings. *Smart Materials and Structures* 24(10) (2015). DOI 10.1088/0964-1726/24/10/105032.
- [14] Babilio, E., Miranda, R., Fraternali, F.: On the kinematics and actuation of dynamic sunscreens with tensegrity architecture. *Frontiers in Materials* 6 (2019). DOI 10.3389/fmats.2019.00007.
- [15] Armstrong, A., Buffoni, G., Eames, D., James, R., Lang, L., Lyle, J., Xuereb, K.: The Al Bahar towers: multidisciplinary design for middle east high-rise, abu dhabi, united arab emirates. *The Arup Journal* 2, 60–73 (2013).
- [16] Karanouh, A., Kerber, E.: Innovations in dynamic architecture. *Journal of Façade Design and Engineering* 3(2), 185–221 (2015). DOI 10.3233/FDE-150040.
- [17] Power Jacks, Rolaram, Electric Linear Actuators. Available at: www.powerjacks.com/perch/resources/brochure/pjlab-rolaram-en-01-1b.pdf. Date accessed: 22 Sept. 2019.
- [18] Park, Sanghoon & Kim, Yura & Jung, Hyosub & Park, Jun-Young & Lee, Naesung & Seo, Yongho. (2017). Energy harvesting efficiency of piezoelectric polymer film with graphene and metal electrodes. *Scientific Reports*. 7. 10.1038/s41598-017-17791-3.
- [19] Matthew N. Silletto, Sang-Jae Yoon and Kazuo Arakawa, Piezoelectric cable macro-fiber composites for use in energy harvesting, *Int. J. Energy Res.* 2015; 39:120–127.
- [20] Nagase, K., Skelton, R.E., Network and vector forms of tensegrity system dynamics, *Mechanics Research Communications*, 2014, 59, 14–25.
- [21] Fabbrocino, F., Carpentieri, G.: Three-dimensional modeling of the wave dynamics of tensegrity lattices. *Composite Structures* 173, 9–16 (2017). DOI 10.1016/j.compstruct.2017.03.102.
- [22] EN 1991-1-4 (2005) (English): Eurocode 1: Actions on structures, Parts 1-4: General actions. Wind actions. [Authority: The European Union Per Regulation 305/2011, Directive 98/34/2011, Directive 98/34/EC, Directive 2004/18/EC].
- [23] Strzemiecki, J. and Hobbs, R. E. Properties of wire rope under various fatigue loadings. CESLIC Report SC6, Civil Engineering Department, Imperial College, London, 1988.
- [24] Holloway F.C. (1997) *Material Characterization of Poly (vinylidene Fluoride): a Thin Film Piezoelectric Polymer*, Montana State University-Bozeman, thesis for the degree Of Master of Science in Mechanical Engineering.
- [25] Grzybek D., Piezoelectric generators: materials and structures. *Pomiary Automatyka Robotyka* 17, 2013. DOI: 10.14313/PAR 200/123.
- [26] Reza Moheimani S.O. & Fleming A.J. (2006) *Piezoelectric Transducers for Vibration Control and Damping. Advances in Industrial Control*. Springer, London. DOI 10.1007/1-84628-332-9.
- [27] G. De Pasquale, 11 - Energy harvesters for powering wireless systems*, Editor(s): Deepak Uttamchandani, In Woodhead Publishing Series in Electronic and Optical Materials, Handbook of Memos for Wireless and Mobile Applications, Woodhead Publishing, 2013, Pages 345–400, ISBN 9780857092717, doi.org/10.1533/9780857098610.2.345.
- [28] Jianguo Cai, Xinyu Wang, Ruiguo Yang, Jian Feng, Mechanical behavior of tensegrity structures with High-mode imperfections, *Mechanics Research Communications*, Volume 94, 2018, Pages 58–63, doi.org/10.1016/j.mechrescom.2018.09.006.
- [29] Yao Chen, Jiayi Yan, Jian Feng, Stiffness contributions of tension structures evaluated from the levels of components and symmetry subspaces, *Mechanics Research Communications*, 2019, 103401, doi.org/10.1016/j.mechrescom.2019.103401.
- [30] Shuo Ma, Xing-Fei Yuan, Akram Samy, Shape optimization of a new tensegrity torus, *Mechanics Research Communications*, Volume 100, 2019, 103396, doi.org/10.1016/j.mechrescom.2019.103396.
- [31] PVWatts® calculator, National Renewable Energy Laboratory, U.S. Dept. of Energy. Available at: <https://pvwatts.nrel.gov/pvwatts.php>. Date accessed: 22 Sept. 2019.
- [32] F. Balduzzi, A. Bianchini, L. Ferrari, Microeolic turbines in the built environment: Influence of the installation site on the potential energy yield, *Renewable Energy* 45 (2012) 163–174.